Tailoring Terminal Groups in Sulfonyl Solvents to Boost Compatibility with Lithium Metal Anodes

Jinmin Wang[a,#], Shuang Wei [b,c,#], Mingming Fang[b]*, Angye Li[d], Qian Zheng[a], Xubing Dong[b], Yuanmao Chen[b], Kang Yuan[b], Xinyang Yue[b,]*, Zheng Liang[b,]*

[a] School of Petrochemical Engineering, Changzhou University, Changzhou 213164, China

[b] Frontiers Science Center for Transformative Molecules, School of Chemistry and Chemical Engineering, Shanghai Jiao Tong University, Shanghai 200240, China

[c] Shanghai TANSUO Testing and Inspection Company, Shanghai 200240, China

[d] Xi'an Jiaotong-Liverpool University, Suzhou 215000, China

* Corresponding authors: 193679@sjtu.edu.cn (M. F.); xinyangyue@sjtu.edu.cn (X.Y.); liangzheng06@sjtu.edu.cn (Z.L.)

[#] These authors contributed equally to this work

Experimental Section

Synthesis of N,N-dimethylsulfamoyl fluoride solvent

Under a dry nitrogen atmosphere, a dry and clean 500 mL four-necked round-bottom flask was charged with 50.0 g of dimethylsulfamoyl chloride and 33.6 g of antimony trifluoride in one portion. The flask was equipped with a mechanical stirrer and a thermometer. The reaction mixture was gradually heated to 60 °C in an oil bath with continuous stirring. After maintaining this temperature for 2 hours, the reaction progress was monitored by thin-layer chromatography (TLC) or gas chromatography (GC). If the reaction was not complete after 24 hours, an additional 5-10 mol% equivalent of antimony trifluoride could be added to facilitate completion. Upon full conversion, the setup was converted to a fractional distillation system under reduced pressure. The fraction boiling at 61-64 °C under the corresponding vacuum was collected as the desired product, N,N-dimethylsulfamoyl fluoride, obtaining an isolated yield of 69.8%.

Synthesis of sulfamoyl fluoride solvent

Step 1: Under a dry nitrogen atmosphere, a dry and clean 1000 mL four-neck round-bottom flask was charged with 198 g of starting material and 100 g of antimony trifluoride in one portion. A 30 cm fractionating column was installed, and the mixture was gradually heated to 95 °C with continuous collection of distillates. Heating was discontinued when the overhead temperature reached 116 °C and no further distillate was observed, affording 143 g of collected fraction.

Step 2: Subsequently, another dry four-neck flask was charged with 286 mL of dichloromethane and the 143 g crude product from the previous step. The mixture was cooled in an ice-water bath to maintain an internal temperature of 0–10 °C, and formic acid was added dropwise, during which exotherm, precipitation of a white solid, and gas evolution were observed. After the addition was complete, the reaction mixture was allowed to warm naturally to ambient temperature, accompanied by vigorous gas release, and stirred overnight at room temperature. The following day, the mixture was heated under reflux for 2 h, after which dichloromethane was removed by atmospheric

distillation until the internal temperature reached 60 °C and no more distillate was collected. The residue was then concentrated under reduced pressure using a water aspirator for 20 min, followed by distillation under reduced pressure with an oil pump, yielding 87 g of the desired fraction as the pure sulfonyl fluoride product. All operations were carried out in a fume hood with appropriate personal protective equipment.

Preparation of electrolytes, electrodes, and cells

The lithium bis(fluorosulfonyl)imide (LiFSI), lithium hexafluorophosphate ($LiPF_6$), and 1,2-Dimethoxyethane (DME) were purchased from Duoduo Chem. The Anhydrous Antimony trifluoride was purchased from Alfa Aesar. The Chlorosulfonyl isocyanate, N, N-dimethyl sulfamoyl chlorine, N,N-Dimethyl trifluoromethane sulfonamide and Formic acid were purchased from TCI. The studied electrolyte was prepared by mixing LiFSI, $LiPF_6$ and DMSF with a molar ratio from 1: 0.1: 3 to 1: 0.1 7, and the three reference electrolytes are LiFSI-1.1DME (with a molar ratio of 1: 1.1), LiFSI/$LiPF_6$-5SF (with a molar ratio of 1:0.1: 5) and CCE ($LiPF_6$-EC/DMC (V/V=3:7)-5 wt% FEC. All electrolytes were dried by molecular sieve before testing to make sure that the water content was less than 2 ppm, which was detected by a coulometric Karl Fischer Titrator. All the following preparation processes were carried out in an Ar-filled glove box, where the moisture and oxygen contents were <0.01 ppm. The working NCM811 cathode was prepared by casting an as-prepared N-methylpyrrolidone (NMP) slurry (NCM811 (HeFei Prospect New Energy Technology Ltd.), acetylene black (AB, Li-400, Denka Co. Ltd.) and polyvinylidene difluoride (PVDF) with a weight ratio of 91.5: 5: 3.5). The slurry was coated on an Al foil (8 μm, DodoChem) and the areal capacity of NCM811 was approximately 4.0 mAh cm^{-2} using an automatic coater (HF-Kejing, MSK-AFA-I). An ultrathin Li foil (Guangdong Canrd New Energy Technology Co. Ltd.) with a thickness of 50 μm was used as the anode in the full cells. All 2032-type coin cells were assembled in the Ar-filled glove box and were fabricated using polyethylene as the separator with 60 μL of electrolyte. The Li||NCM811 pouch cells were purchased by Beijing Li-Volt Energy Technology Co., Ltd.

Electrochemical measurement

The Li||NCM811 full cells were activated at 0.1 C for the first two formation cycles and 0.2 C for the next five cycles, and then cycled at 0.3 C charge and 0.5 C discharge with a cut-off voltage range of 2.5 ~ 4.5 V (1 C: 230 mAh g^{-1}). The long-term cycling and rate tests of the cells were performed using a Neware tester (CT-4008) and a LAND CT2001A battery tcarboxylate (Wuhan, China) at 30 °C. For the rate test, the full cells were charged and discharged at different rates after formation with a voltage range of 2.5~4.5 V. Electrochemical impedance spectroscopy (EIS) measurements were performed in a frequency range from 100 kHz to 0.1 Hz using a voltage amplitude of 10 mV (VMP300, Bio-Logic). Cyclic voltammetry (CV) measurements were carried out by a potentiostat (BioLogic, MPG-2) with a scanning speed of 0.2 mV s^{-1}.

Characterization

The Li^+ solvation structure was meticulously examined utilizing a Raman spectrometer (Horiba Lab RAM HR) with an excitation wavelength of 532 nm, alongside a nuclear magnetic resonance (NMR) spectrometer (Bruker AV400, Switzerland). All electrolyte samples subjected to testing were contained within sealed capillary tubes. NMR spectra were acquired using deuterated acetone (acetone-d6) as the solvent. The chemical shift values (in ppm) were calibrated with DMSO as an external reference, facilitating the NMR spectral analysis for ^{1}H (400 MHz), ^{13}C (400 MHz) and ^{7}Li (156 MHz). The cycled NCM811 and Li electrodes were procured by disassembling the cycled cells within an inert glove box. Prior to characterization, all solid samples were meticulously washed three times with dimethyl carbonate (DMC). Morphological analysis was conducted using high-resolution scanning electron microscopy (SEM, Hitachi, Regulus 8230). High-angle annular dark-field scanning transmission electron microscopy (HAADF-STEM) images were obtained via an FEI (now Thermo Fisher) spherical aberration corrected Titan ChemiSTEM microscope (USA). The chemical structure was elucidated through X-ray photoelectron spectroscopy (XPS, ESCALAB Xi^+), employing Al-Kα radiation. To mitigate surface charge accumulation on the samples, a charge neutralizer was utilized. Calibration of binding energy was performed using

the C−C peak at 284.8 eV. X-ray photoelectron spectroscopy (XPS) depth profiling was achieved via Ar^+ sputtering at 1 kV, with the sputtering rate for XPS depth profiling calibrated on the TaO_2 surface approximating 0.04 nm s^{-1}. Subsequently, the samples were transported from the Ar-filled glove box to the instrumental chambers using a specialized "Sample Transfer Vessel," ensuring they remained free from air exposure. The Li||NCM811 pouch cell (1 Ah) was charged to 4.5 V after two activation cycles (2.5–4.5 V, 0.1 C) and then penetrated with a nail (diameter = 3 mm) at a piercing speed of 80 mm s^{-1}.

Theoretical calculations

In this study, MD simulations were performed in GROMACS using the General Amber Force Field (GAFF). Topology files and bonded and Lennard-Jones parameters were generated by using the Autoff while the RESP atomic charges from Multiwfn3.8 program were used. The cutoff for the Lennard-Jones potential was set to 12 Å. The long-range Coulombic interactions were counted by a particle–particle particle-mesh. The initial periodic systems were set up using PACKMOL. All ions and molecules were inserted in an initial cube box with 10 nm sides. In the equilibrium stage of the system, the energy of the simulated system was minimized by the conjugate gradient method first, then the equilibrium simulation was carried out under NPT ensemble for 10 ns. Finally, the simulation was continued for 20 ns with NVT ensemble and data were collected. Only the final 10-ns trajectory was sampled for the analysis of radial distribution function and solvent-solute interaction environments.

All the molecules were optimized using Gaussian with the three-parameter empirical formulation B3LYP for the exchange-correlation density-functional energy in conjunction with the basis set of 6-311+G(d,p), and then the energy calculations of molecules were evaluated at the B3LYP/6-311+G(d,p) level as well. A dispersion correction was also considered using the Becke-Johnson damping function. The solvent-solute interaction was considered with the universal solvation model of SMD. Frequency analysis was performed to ensure the ground state of molecular structures.

The binding energy was calculated by subtracting the reactant energies from the complex energy.

The AIMD calculations, based on the DFT as employed in the CP2K, are carried out with the Perdew-Burke-Ernzerh of formulation of the generalized gradient approximation. The core electrons were described by the Gaussian and plane-wave basis and the convergence criterion for energy is $1.0E^{-8}$ eV. The convergence criterion of self-consistent field loop based on orbital transformation (OT) method was set as 1.0E-4 eV. Besides, a long-range dispersion-correction DFT-D3 was involved for all calculations. A 3 × 3 × 1 supercell of cubic phase lithium is cleaved to generate (100) crystallographic plane to represent a positive electrode surface. To avoid interactions between neighboring images, a vacuum region of 25 Å is implemented. 2 LiFSI and 6 DMSF are inserted in the vacuum space randomly to simulate the electrolyte environment. AIMD simulation for 100 ps at 300 K is performed with a timestep of 1 fs, where the temperature is regulated by the NVT ensemble with the Nosé-Hoover thermostat. The VESTA program is utilized to visualize the crystal structures.

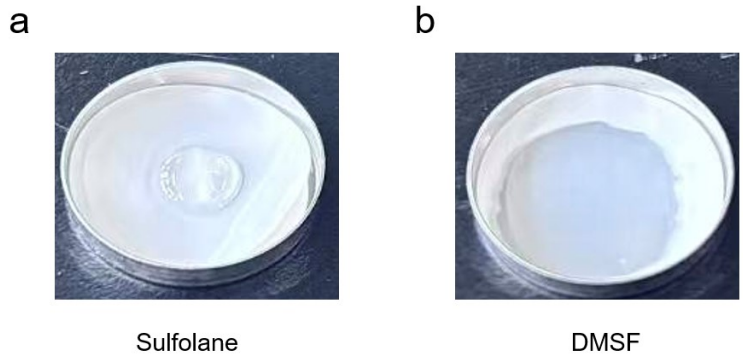

Fig. S1 (a) Comparison of the separator wettability of sulfolane and functionalized DMSF solvents. (a) Sulfolane. (b) DMSF.

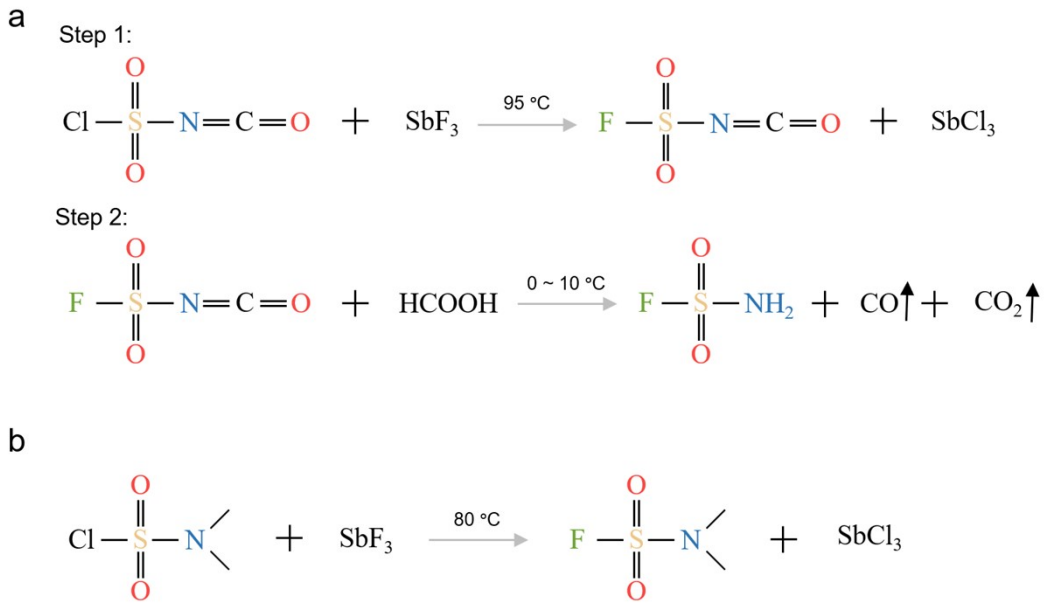

Fig. S2 (a) Synthesis scheme illustration of the sulfamoyl fluoride. (b) Synthesis scheme illustration of the N,N-dimethylsulfamoyl fluoride.

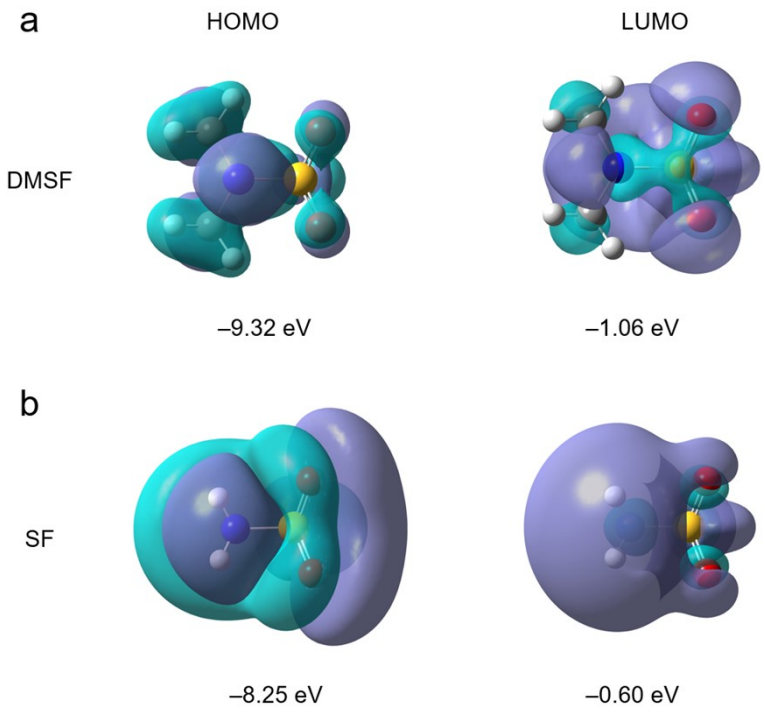

Fig. S3 Comparison of the highest occupied molecular orbital (HOMO)-lowest unoccupied molecular orbital (LUMO) energy levels for (a) DMSF and (b) SF.

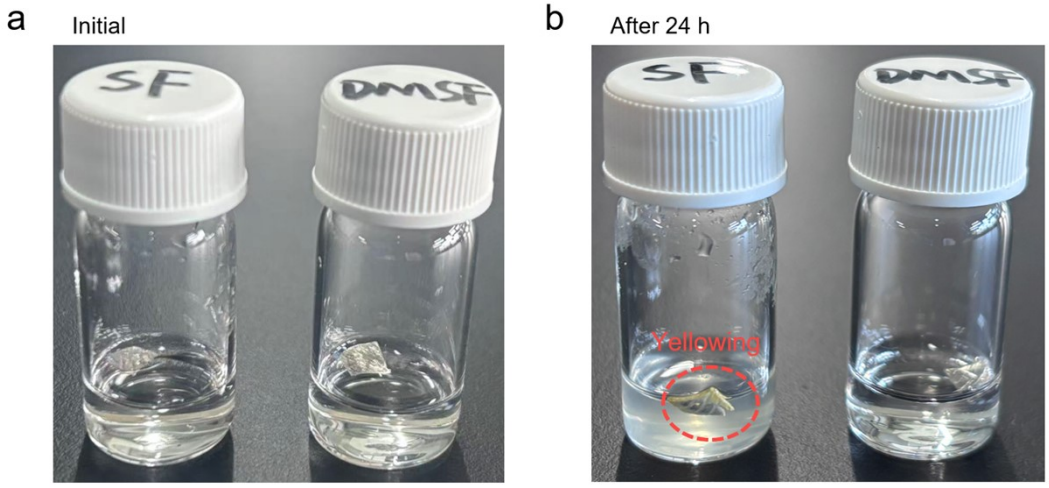

Fig. S4 (a) The soaking experiment of Li metal in the FSI/PF-SF and FSI/PF-DMSF electrolytes after different time. a) initial, (b) after 24 h.

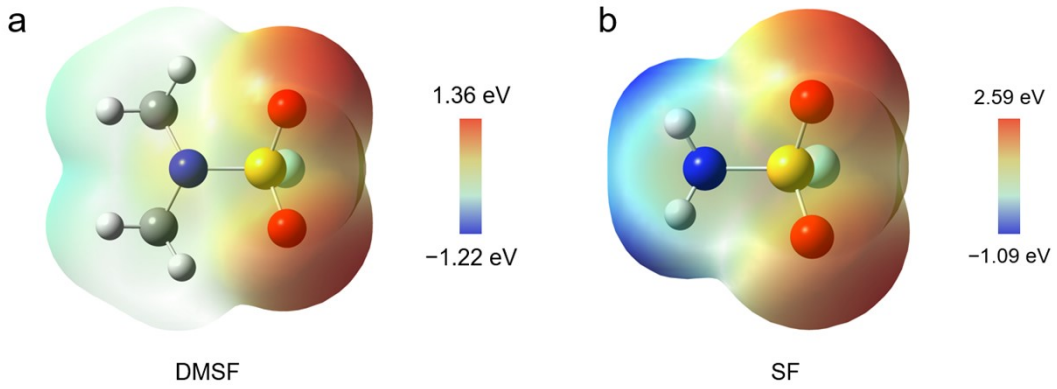

Fig. S5 The electrostatic potential (ESP) map of (a) DMSF and (b) SF.

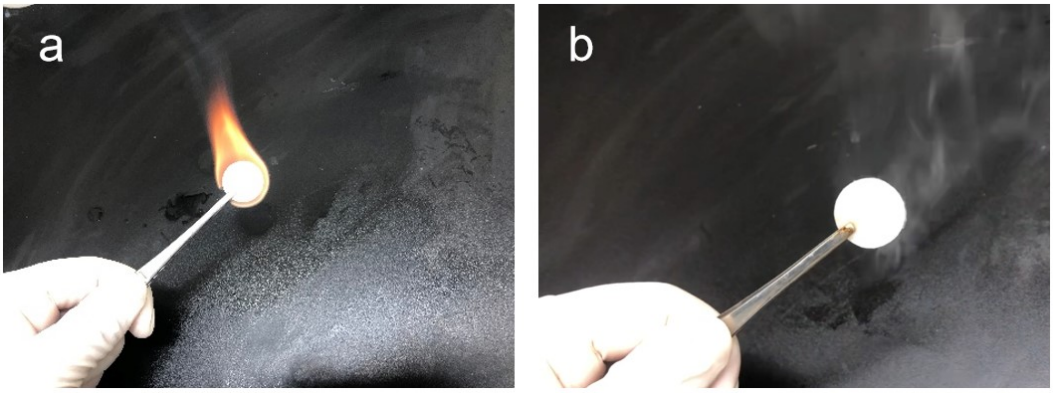

Fig. S6 Flame retardance tests of (a) CCE and (b) FSI/PF-DMSF electrolytes.

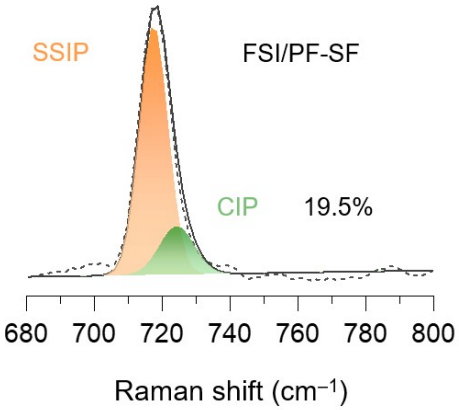

Fig. S7 Fitted Raman spectra of FSI/PF-SF electrolytes in the wavelength range from 680 to 800 cm^{-1}.

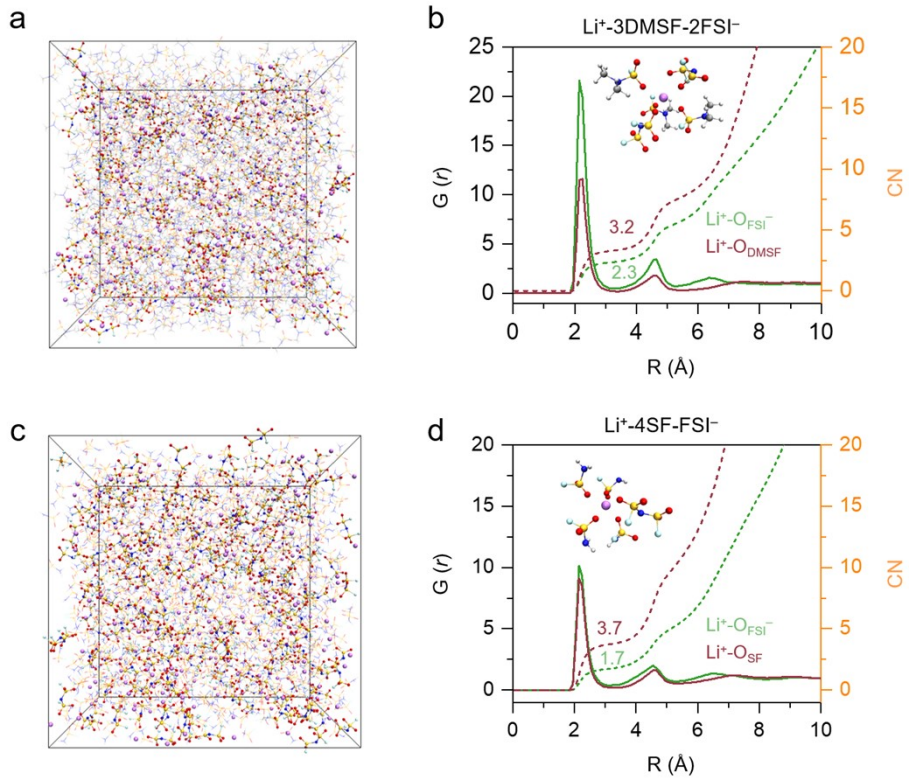

Fig. S8 (a, c) MD simulation snapshots of (a) FSI/PF-DMSF and (c) FSI/PF-SF electrolytes. (b, d) RDF (solid lines) and coordination number (dashed lines) of Li^+-Osolvent and Li^+-ODFOB$^-$ in (b) FSI/PF-DMSF and (d) FSI/PF-SF electrolytes. The inset shows the primary solvation structural configuration.

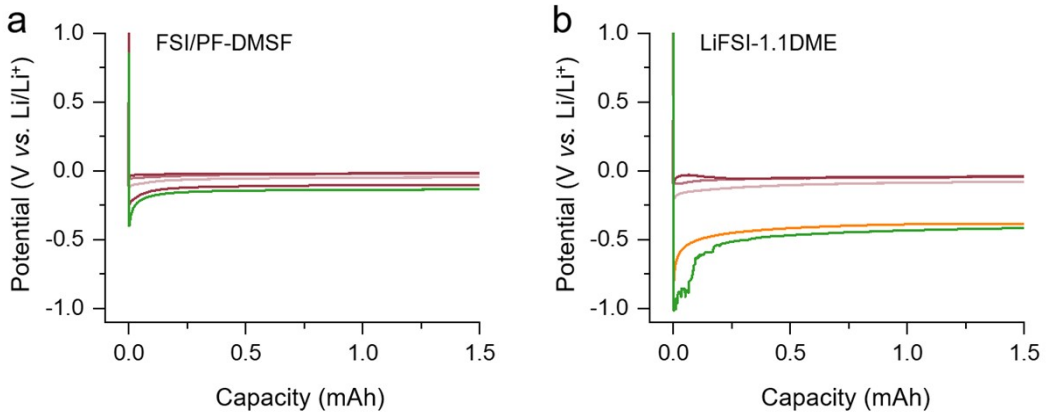

Fig. S9 (a, b) The plating curves at different current densities using different electrolytes. (a) FSI/PF-DMSF electrolyte, (b) LiFSI-1.1DME electrolyte.

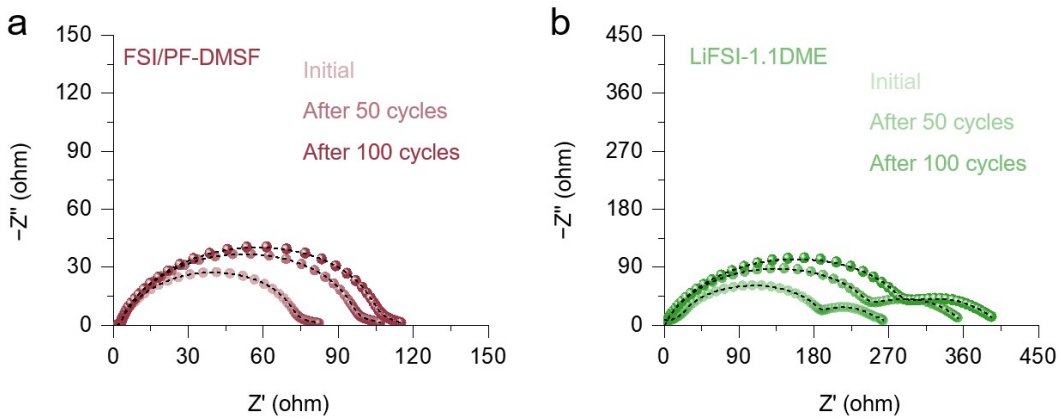

Fig. S10 The electrochemical impedance spectroscopy spectra of the Li symmetric cells using (a) FSI/PF-DMSF and (b) LiFSI-1.1DME electrolytes at different cycles.

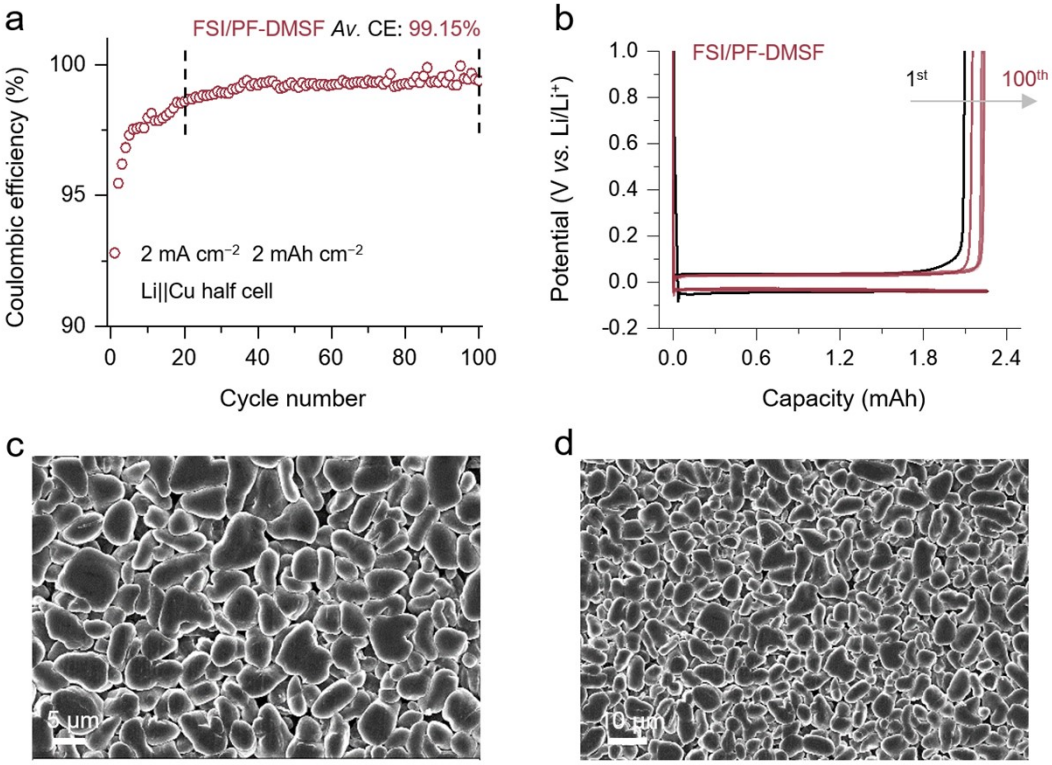

Fig. S11 (a) CEs of Li stripping/plating as a function of cycle number tested in Li||Cu electrochemical cells under 2 mA cm^{-2} and 2 mA h cm^{-2}. (b) The selected voltage profiles for Li||Cu plating/stripping in FSI/PF-DMSF. (c, d) Top-view SEM images of deposited Li using the FSI/PF-DMSF under 2 mA cm^{-2}.

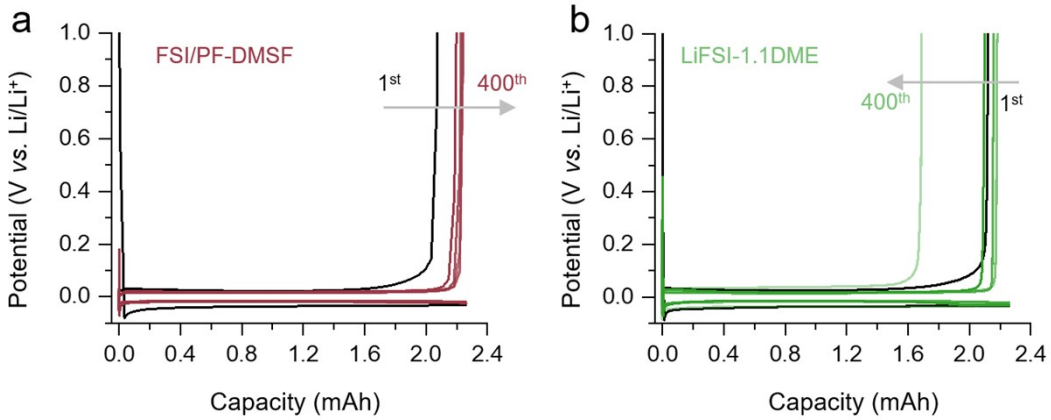

Fig. S12 The Li plating/stripping profiles in (a) FSI/PF-DMSF and (b) LiFSI-1.1DME electrolytes at different cycles. The first cycle (black lines) shows the initial Coulombic efficiency.

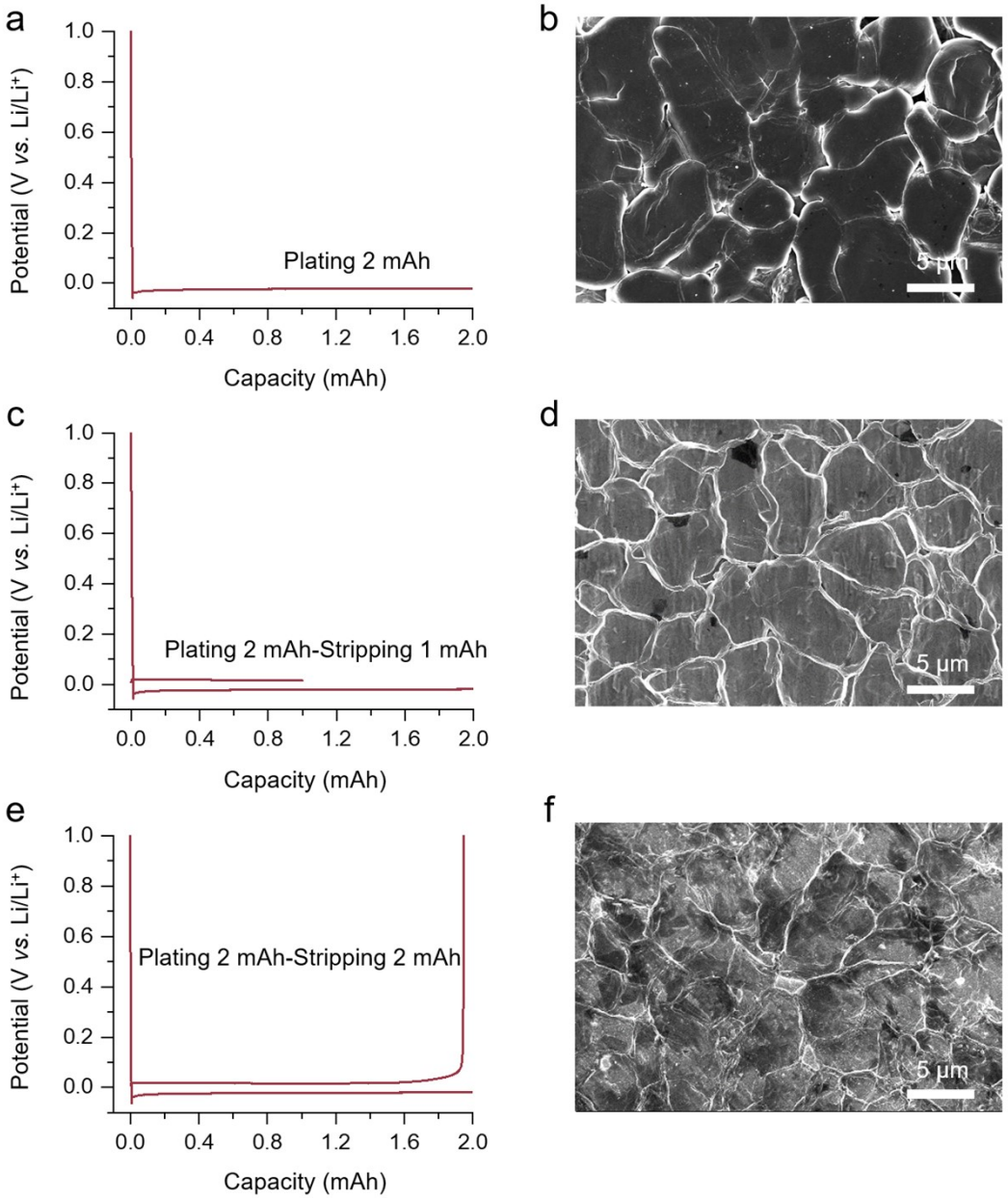

Fig. S13 (a-f) Morphological evolution of Li plating/stripping in FSI/PF-DMSF across cycling stages. (a, b) Plating 2 mAh, (a, b) Plating 2 mAh-Stripping 1 mAh, (e, f) Plating 2 mAh-Stripping 2 mAh.

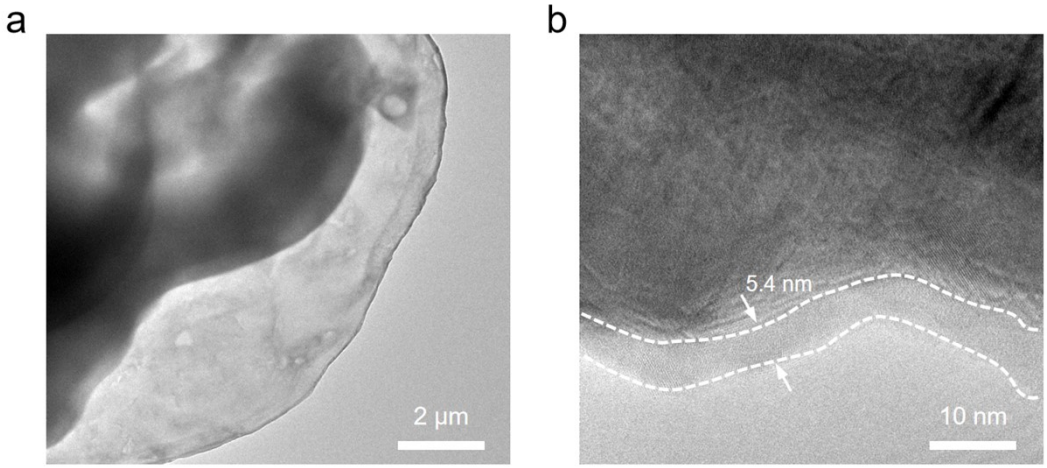

Fig. S14 (a) Cryo-TEM and (b) HRTEM images of the SEI formed in FSI/PF-DMSF.

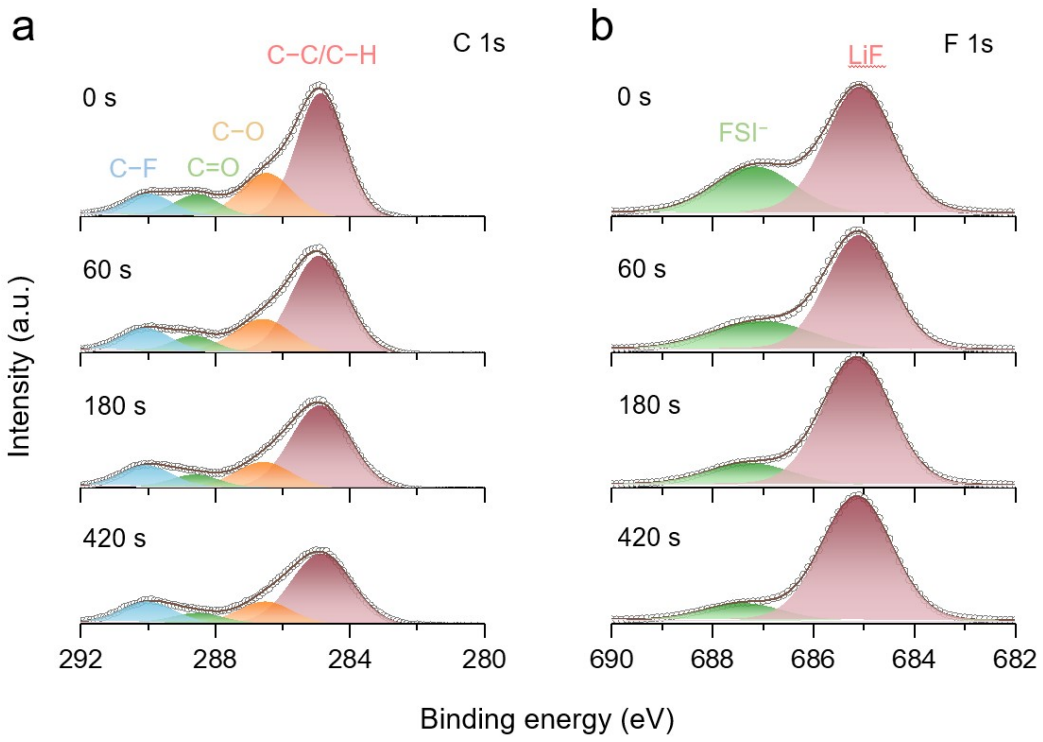

Fig. S15 XPS spectra of (a) C 1s and (b) F 1s on the Li metal interphase cycled in CCE.

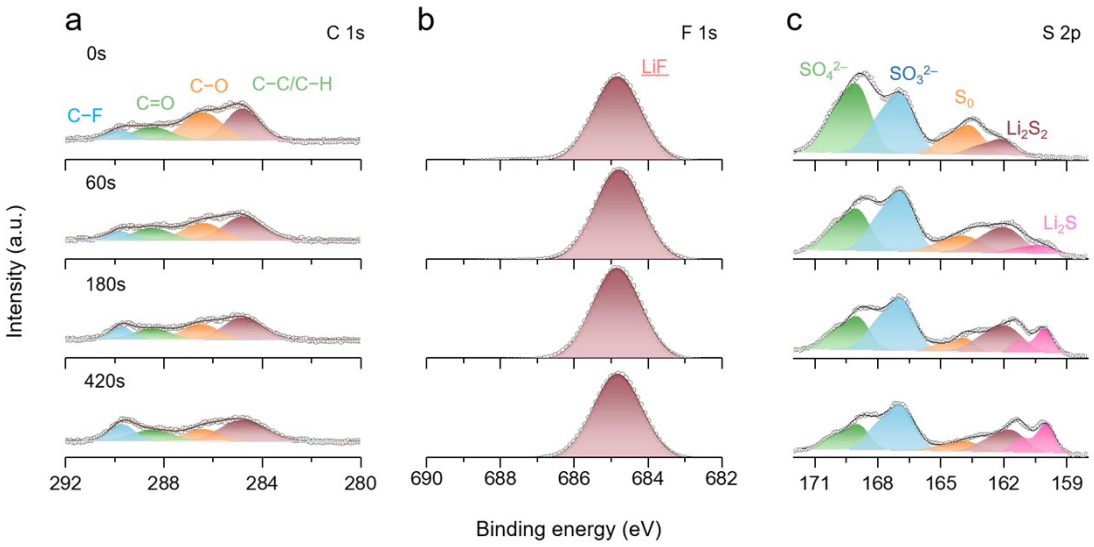

Fig. S16 XPS spectra of (a) C 1s, (b) F 1s and (c) S 2p on the Li metal interphase cycled in LiFSI-1.1DME.

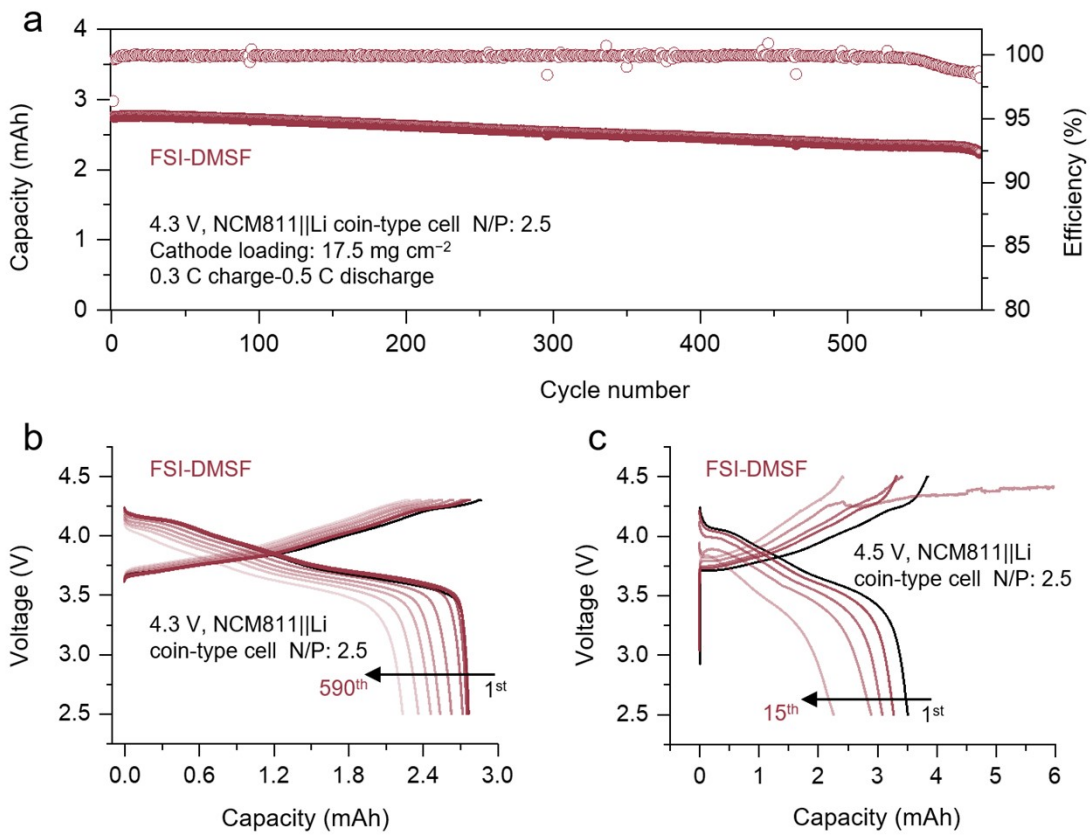

Fig. S17 (a) Long-cycling performance of 4.3 V charged Li||NCM811 coin cell in FSI-DMSF, (b) The charge–discharge curves of the cell using FSI-DMSF electrolyte in (a). (c) The charge–discharge curves of the cell using FSI-DMSF electrolyte at 4.5 V.

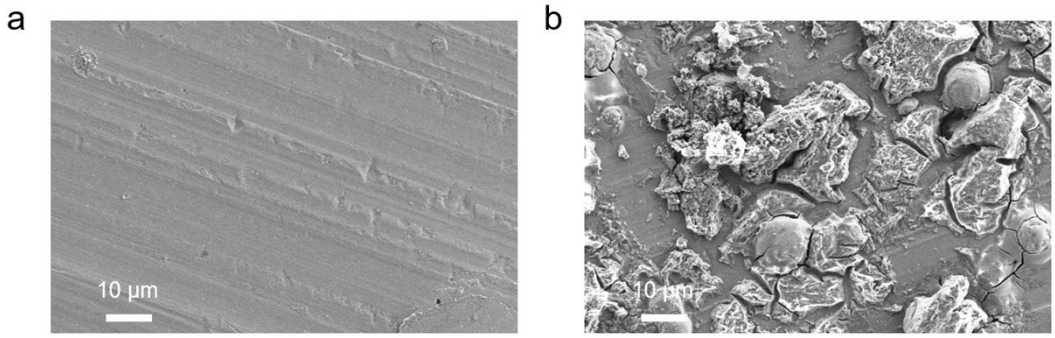

Fig. S18 The SEM images of the cycled Al foil obtained from the CA tests using (a) FSI/PF-DMSF and (b) FSI-DMSF electrolytes.

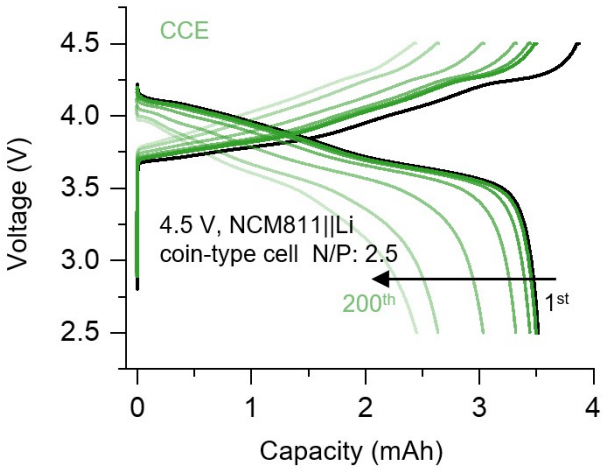

Fig. S19 The charge–discharge curves of 4.5 V charged Li||NCM811 coin cell in CCE.

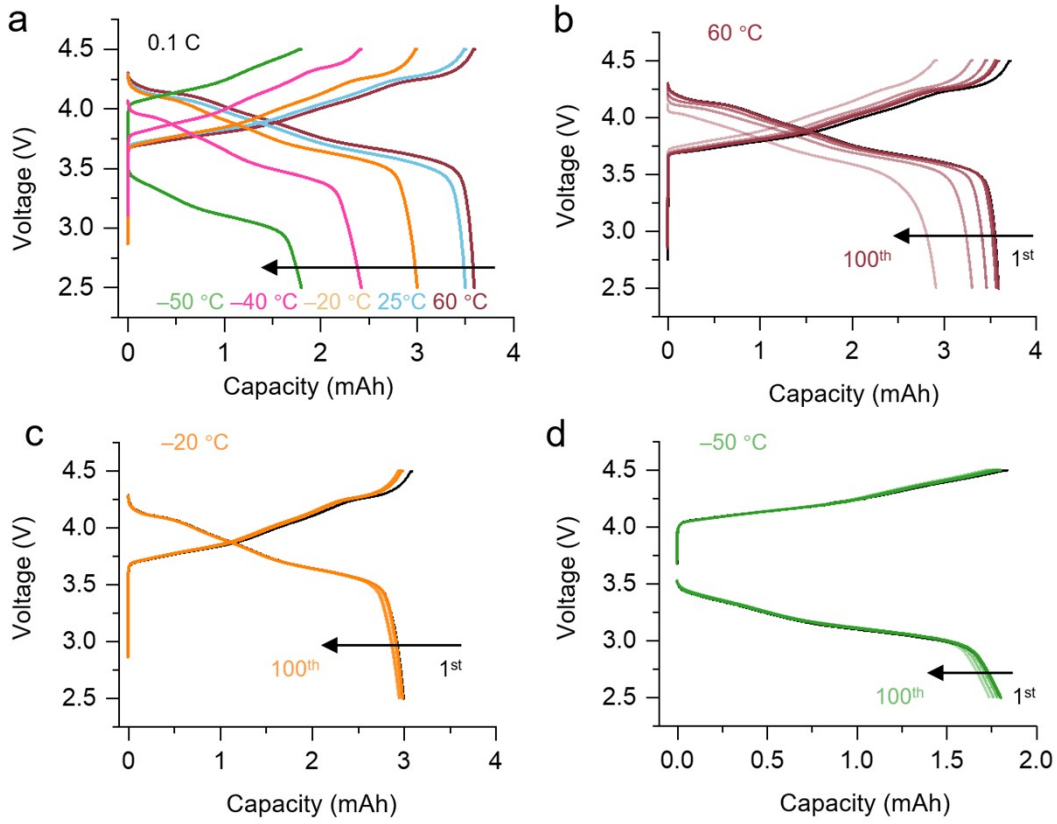

Fig. S20 (a) The charge–discharge curves of Li||NMC811 cells using FSI/PF-DMSF electrolyte at different temperatures. (b-d) The curves of FSI/PF-DMSF electrolyte at (c) 60 °C, (d) −20 °C, and (e) −50 °C.

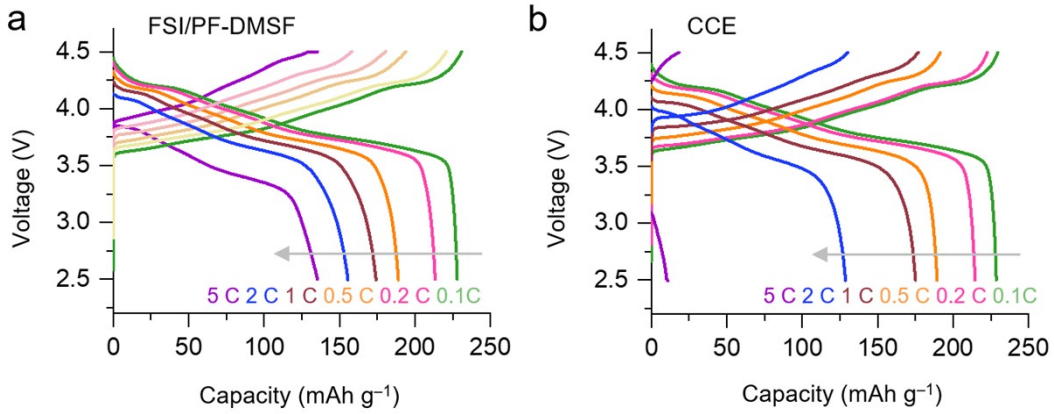

Fig. S21 The Charge–discharge curves of Li||NCM811 cells using FSI/PF-DMSF and CCE electrolytes at different rates.

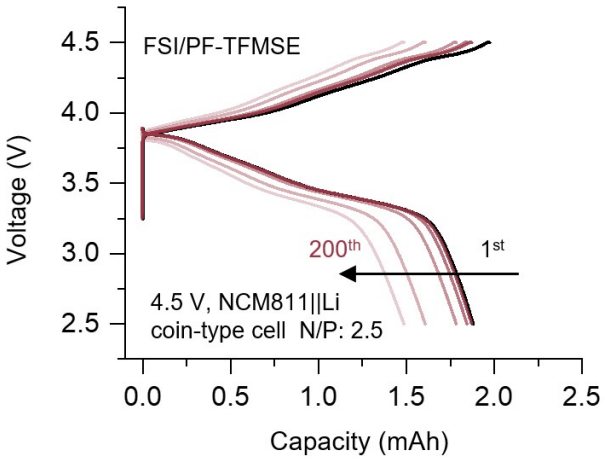

Fig. S22 The charge–discharge curves of Li||NMC811 cells using FSI/PF-DMSF electrolyte at 5 C.

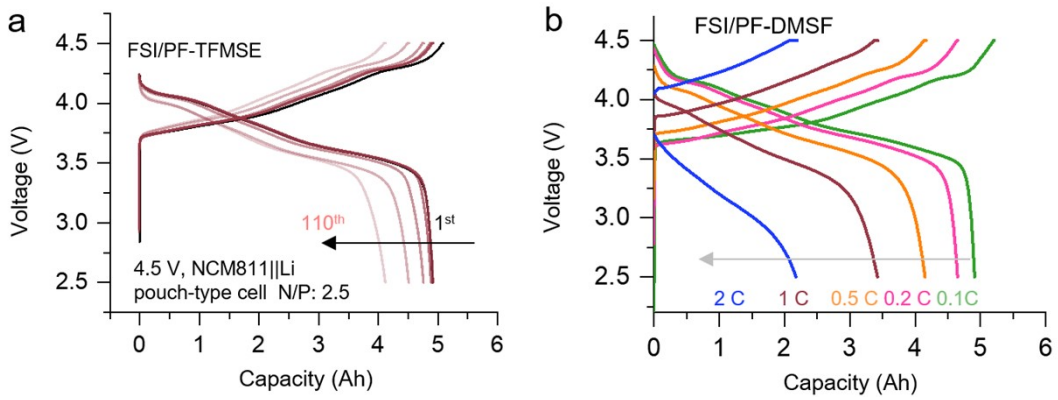

Fig. S23 (a) The charge–discharge curves of Li||NMC811 pouch cells using FSI/PF-DMSF electrolyte. (b) The Charge–discharge curves of Li||NCM811 pouch cells using FSI/PF-DMSF at different rates.

Fig. S24 Photographs images of a cycled Li||NCM811 pouch cell with FSI/PF-DMSF during nail penetration tests.

Table S1. Ionic conductivity of FSI/PF-SF, FSI/PF-DMSF, and FSI/PF-DMSTF electrolytes at different temperatures.

Electrolytes	**Ionic conductivity ($mScm^{-1}$)**						
	−50 ℃	−40 ℃	−20 ℃	0 ℃	25 ℃	60 ℃	80 ℃
FSI/PF-SF	0.2	1.9	3.1	3.9	5.4	7.8	10.2
FSI/PF-DMSF	0.12	1.5	2.3	3.3	4.8	7.2	9.6
FSI/PF-DMSTF	-	0.008	0.12	0.9	1.6	4.2	6.7

Table S2. Parameters of 5-Ah Li||NCM811 pouch cells.

Pouch cell structure	Parameter	Value
Cathode	Specify capacity	230 mAh g^{-1}
	Areal capacity	4.0 mAh cm^{-2}
	Areal weight	17.8 mg cm^{-2}
	Number of layers	13
	Electrolyte size	Length:80 mm, Wide: 60 mm
	Total weight	22.2 g
Li metal	Thickness (double sides)	100 μm
	Electrode size	Length:82 mm, Wide: 62 mm
	Number of layers	14
	Total weight	3.8 g
Electrolyte	E/C ratio	1 g Ah^{-1}
	Total weight	5.0 g
Al foil	Thickness	10 μm
	Total weight	1.6 g
Separator	Total weight	0.5 g
Tab	Total weight	0.1 g
Package	Total weight	2.2 g
Cell	Total weight	35.4 g
	Average voltage	3.9 V
	Energy density	539.8 Wh kg^{-1}

Note of Table S2: Energy density calculation method:

The total weight of 4.5 V Li||NCM811 pouch cell was 35.4 g, and the average output voltage was 3.9 V. Thus, the calculated energy density of 4.5 V-level graphite||NCM811pouch cells was 539.8 Wh kg^{-1} (= 4.9 Ah × 3.9 V/0.0354 kg).

Abbreviation	Electrolyte	Anode|| Cathode	Cell specifications	Cell capacity	Energy density (Wh kg^{-1})	Capacity retention	Work voltage (V)	Reference
PFOA-Li	1 M $LiPF_6$-EMC/DEC+10%FEC	Li||NCM9055	N/P = 2.4 E/C = 1.12 g Ah^{-1}	5.8 Ah	518	75% (100 cycles)	4.3 V	1
LiFSI-TEP/BTFE	1.2M LiFSI-TEP/BTFE (1:2 by vol.)	Li||NCM622	N/P = 2.6 E/C = 3.0 g Ah^{-1}	1.0 Ah	300	83% (200 cycles)	4.3 V	2
LiFSI–DME/TTE	1.5 M LiFSI–DME–TTE	Li||NCM622	N/P = 1.1 E/C = 2.4 g Ah^{-1}	2.0 Ah	350	81% (500 cycles)	4.4 V	3
DMTMSA	1 m LiFSI/DMTMSA	Li||NCM811	N/P = 2.9 E/C = 2.3 g Ah^{-1}	4.86 mAh	353	88% (90 cycles)	4.7 V	4
LiFEA	LiFEA/$LiNO_3$/$LiPF_6$-EC/DEC (v/v = 1:1)	Li||NCM811	N/P = 2.7 E/C = 2.8 g Ah^{-1}	0.42 Ah	310	81% (100 cycles)	4.3 V	5
Bilayer/P–F SEI	LiFSI-0.16TO-1.80DME-2.00HFE	Li||NCM811	N/P = 1.8 E/C = 2.1 g Ah^{-1}	5.3 Ah	440	91.7% (130 cycles)	4.3 V	6
CIPA	LiFSI-EGBE-TTE	Li||NCM90	N/P = 1.5 E/C = 1.12 g Ah^{-1}	19.0 Ah	505.9	91% (130 cycles)	4.3 V	7
TMEE	2 M LIFSI-TMEE	Li||NCM811	N/P = 0.5 E/C = 1.33 g Ah^{-1}	14.0 Ah	512	90% (100 cycles)	4.4 V	8
E-Pry2(2)FSI	1.5 M LiFSI-Pyr2(2)FSI/DME (1:2 mol%)	Li||NCM811	N/P = 2.0 E/C = 2.0 g Ah^{-1}	0.49 Ah	313.4	87.4% (150 cycles)	4.3 V	9
FEC/CTAC/TPFPB	1 M $LiPF_6$-EC/EMC/DMC+FEC/CTAC/TPFPB	Li||NCM83	N/P = 1.54 E/C = 1.1 g Ah^{-1}	7.41 Ah	522	92% (178 cycles)	4.4 V	10
C-DHCE	LiFSI-1.2DME-FB/F3B/TTE	Li||NCM622	N/P = 1.04 E/C = 1.7 g Ah^{-1}	2.95 Ah	518	92% (107 cycles)	4.6 V	11
FSNMD	1.5 M LiFSI-FSNDM	Li||NCM811	N/P = 1.95 E/C = 1.02 g Ah^{-1}	5.97 Ah	495.5	80% (150 cycles)	4.3 V	12
DMSF	1.6 M LiFSI/PF-DMSF	Li||NCM811	N/P = 2.5 E/C = 1.0 g Ah^{-1}	4.59 Ah	539.8	83% (110 cycles)	4.5 V	Our work

Table S3. Comparison of our work with recent electrolyte works on graphite||NCM811, Si||NCM811 and Li||NCM811 pouch cells.

References

[1] Z. Jiang, J. Liu, K. Yue, M. Pang, Y. Peng, C. Luo, Z. Yao, T. Pan, Y. Wang, Y. Li, Q. Guo, C. Zheng, W. Sun, X. Tao, S. Liu, *Energy Environ. Sci.* 2025, **18**, 9240-9253.

[2] C. Niu, H. Lee, S. Chen, Q. Li, J. Du, W. Xu, J.-G. Zhang, M. S. Whittingham, J. Xiao, J. Liu, *Nat. Energy* 2019, **4**, 551-559.

[3] C. Niu, D. Liu, J. A. Lochala, C. S. Anderson, X. Cao, M. E. Gross, W. Xu, J.-G. Zhang, M. S. Whittingham, J. Xiao, J. Liu, *Nat. Energy* 2021, **6**, 723-732.

[4] W. Xue, M. Huang, Y. Li, Y. G. Zhu, R. Gao, X. Xiao, W. Zhang, S. Li, G. Xu, Y. Yu, P. Li, J. Lopez, D. Yu, Y. Dong, W. Fan, Z. Shi, R. Xiong, C.-J. Sun, I. Hwang, W.-K. Lee, Y. Shao-Horn, J. A. Johnson, J. Li, *Nat. Energy* 2021, **6**, 495-505.

[5] Y. Xia, P. Zhou, X. Kong, J. Tian, W. Zhang, S. Yan, W.-h. Hou, H.-Y. Zhou, H. Dong, X. Chen, P. Wang, Z. Xu, L. Wan, B. Wang, K. Liu, *Nat. Energy* 2023, **8**, 934-945.

[6] Q.-K. Zhang, X.-Q. Zhang, J. Wan, N. Yao, T.-L. Song, J. Xie, L.-P. Hou, M.-Y. Zhou, X. Chen, B.-Q. Li, R. Wen, H.-J. Peng, Q. Zhang, J.-Q. Huang, *Nat. Energy* 2023, **8**, 725-735.

[7] Y. Jie, S. Wang, S. Weng, Y. Liu, M. Yang, C. Tang, X. Li, Z. Zhang, Y. Zhang, Y. Chen, F. Huang, Y. Xu, W. Li, Y. Guo, Z. He, X. Ren, Y. Lu, K. Yang, S. Cao, H. Lin, R. Cao, P. Yan, T. Cheng, X. Wang, S. Jiao, D. Xu, *Nat. Energy* 2024, **9**, 987-998.

[8] G. Zhang, T. Zhang, Z. Zhang, R. He, Q. Wang, S.-S. Chi, Y. Cui, M. D. Gu, Z. Liu, J. Chang, C. Wang, K. Xu, Y. Deng, *Nat. Commun.* 2025, **16**, 4722.

[9] J. Jang, C. Wang, G. Kang, C. Han, J. Han, J.-S. Shin, S. Ko, G. Kim, J. Baek, H.-T. Kim, H. Lee, C. B. Park, D.-H. Seo, Y. Li, J. Kang, *Nature Energy* 2025, **10**, 502-512.

[10] T. Tang, C. Sun, Y. Li, M. Tong, J. Lu, C. Lai, *Angew. Chem. Int. Ed.* 2024, **64**, e202417471.

[11] J. Peng, H. Zhang, Z. Zeng, H. Zhang, H. Pei, Q. Wu, Y. Shen, R. Guo, S. Cheng, J. Xie, *Adv. Mater.* 2025, e09109.

[12] Z. Yu, H. Wang, X. Kong, W. Huang, Y. Tsao, D. G. Mackanic, K. Wang, X. Wang, W. Huang, S. Choudhury, Y. Zheng, C. V. Amanchukwu, S. T. Hung, Y. Ma, E. G. Lomeli, J. Qin, Y. Cui, Z. Bao, *Nat. Energy* 2020, **5**, 526-533.

[13] L.-Q. Wu, Z. Li, H. Li, J.-Y. Zhang, Y. Li, S.-X. Ren, Z.-Y. Fan, X.-T. Wang, K. Li, Z. Liu, J. Zhang, J.-C. Yang, Y.-W. Li, S.-H. Bo, Q. Zhao, *J. Am. Chem. Soc* 2025, **147**, 16506-16521.